Ore Geology Reviews 157 (2023) 105426

Contents lists available at ScienceDirect

Ore Geology Reviews

journal homepage: www.elsevier.com/locate/oregeorev

Cd isotope constraints on metal sources of the Zhugongtang Zn–Pb deposit, NW Guizhou, China

Wenrui Song [a,b], Lisheng Gao [a], Chen Wei [c], Yunzhu Wu [a,b], Hanjie Wen [d,e], Zhilong Huang [a], Jiawei Zhang [f], Xiaocui Chen [g], Yuxu Zhang [a], Chuanwei Zhu [a,*]

[a] State Key Laboratory of Ore Deposit Geochemistry, Institute of Geochemistry, Chinese Academy of Sciences, Guiyang 550081, China
[b] School of Earth Resources, China University of Geosciences, Wuhan 430074, China
[c] Helmholtz–Zentrum Dresden–Rossendorf, Helmholtz Institute Freiberg for Resource Technology, Freiberg 09599, Germany
[d] School of Earth Sciences and Resources, Chang'An University, Xi'an 710054, China
[e] College of Earth and Planetary Sciences, University of Chinese Academy of Sciences, Beijing 100049, China
[f] Guizhou Geological Survey, Bureau of Geology and Mineral Exploration and Development of Guizhou Province, Guiyang 550081, China
[g] Guizhou Institute of Technology, Guiyang 550002, China

ARTICLE INFO

Keywords:
Cd isotopes
Zn/Cd ratios
Metal sources
Zhugongtang Zn–Pb deposit

ABSTRACT

The Sichuan–Yunnan–Guizhou metallogenic province (SYGMP) includes > 400 Zn − Pb deposits and prospects, eight of which are large-scale deposits with large reserves of critical metals such as Cd and Ge, including the Huize Zn − Pb − Cd − Ge and Daliangzi Zn–Pb–Ge–Cd deposits. The newly discovered Zhugongtang Zn − Pb deposit is a super-large deposit with Zn–Pb reserves of > 3 Mt. Its geochemical features are similar to those of the Huize deposit, with similar sulfide $\delta^{34}S$ values and concentrations of critical elements in sphalerite (e.g., Cd and Ge). However, the two deposits have different host strata, and it remains unclear as to whether they have similar oregenesis. In this study, $\delta^{114/110}Cd$ values and major- and trace-element compositions of sphalerites collected from a drill-core and tunnels of the Zhugongtang deposit were determined in an investigation of metal sources. Drill-core samples were impure and exhibited strong correlation ($R^2 = 0.89$) between Zn and Cd contents. For samples from mining tunnels, the Cd and Fe contents of selected sphalerites were positively correlated, especially yellow sphalerites ($R^2 = 0.76$). Cadmium is likely hosted in sphalerite by the substitution mechanism of (Fe^{2+}, Cd^{2+}) ↔ Zn^{2+}. The $\delta^{114/110}Cd$ values of all samples ranged from − 0.43 ‰ to 0.06 ‰. Based on Zn/Cd ratios, and excluding geochemical processes that may have caused the variable Cd isotopic compositions, we suggest that the metal sources of the deposit were derived from the mixing of sedimentary and basement rocks. This model is supported by the strong relationship between the $\delta^{114/110}Cd$ and 1/Cd values of sphalerites from 11 typical Zn–Pb deposits in the SYGMP ($R^2 = 0.81$). The quantification of metal contributions of source rocks indicates that deposits derived mainly from sedimentary rocks generally have relatively low sphalerite Ge contents and small Ge reserves, whereas those derived mainly from basement rocks have higher Ge contents and larger Ge reserves. This study provides a new model for explaining the enrichment of critical metals in Zn–Pb deposits of the SYGMP, thus extending the applications of Cd isotopes in hydrothermal systems.

1. Introduction

With current advances in mass spectrometry, it is possible to obtain precise and accurate data for minor changes in the metal isotopic compositions of geological samples, thus aiding the understanding of geological processes (Craddock and Dauphas, 2011; Prytulak et al., 2013; Zhu et al., 2013a; An and Huang, 2014; Millet and Dauphas, 2014; Zhu et al., 2015; Blum and Johnson, 2017; Lu et al., 2017; Teng et al., 2017; Lehmann et al., 2022; Wei et al., 2022). Stable isotopes of metals such as Zn, Cd, Mo, Cu, and Fe are thus becoming important geochemical tools in the understanding of different geological environments (Anbar and Rouxel, 2007; Fan et al., 2007; Wen et al., 2007, 2009; Liu et al., 2015; Yang et al., 2021; Leybourne et al., 2022), particularly in tracing ore genesis (e.g., Mondillo et al., 2018; Li et al., 2019; Cai et al., 2020; Wang et al., 2021; Spry et al., 2022). Most hydrothermal deposits are rich in Cd, the stable isotopes of which have proved useful in

* Corresponding author.
E-mail address: zhuchuanwei@mail.gyig.ac.cn (C. Zhu).

https://doi.org/10.1016/j.oregeorev.2023.105426
Received 3 March 2023; Received in revised form 28 March 2023; Accepted 29 March 2023
Available online 31 March 2023

tracking sources of different types of deposit, including Mississippi Valley type (MVT), volcanic-hosted massive sulfide (VMS), and skarn deposits (Zhu et al., 2013b; 2016; 2017; Wen et al., 2016; Yang et al., 2022a). Low-temperature MVT deposits have more isotopic fractionation ($\delta^{114/110}$Cd = 0.32 ‰ ± 0.31 ‰) than magma-related deposits (e.g., skarn and VMS deposits: $\delta^{114/110}$Cd = 0.04 ‰ ± 0.16 ‰), with sphalerite inheriting the Cd isotopic signatures of source beds (Wen et al., 2016). Zn–Cd–S sulfides of the Xiaobaliang VMS deposit, which underwent strong biological activity, are enriched in light Cd isotopes with $\delta^{114/110}$Cd values of − 0.74 ‰ to − 0.08 ‰ (cf. igneous rocks, $\delta^{114/110}$Cd = ~0‰), suggesting that biological activity recorded by Cd isotopes likely played an important role in the mineralization of VMS systems (Yang et al., 2022a). The Zhaxikang and Keyue Sb–Pb–Zn–Ag deposits of the North Himalayan Metallogenic Belt are separated only by a regional fault, and there is a temporally decreasing trend in $\delta^{114/110}$Cd values from ore-mineralization stage II, with mean $\delta^{114/110}$Cd values for the two deposits of − 0.23 ‰ and 0.05 ‰, to stage III, with mean values of − 0.29 ‰ and − 0.35 ‰, respectively. This implies Rayleigh fractionation associated with the vapor–liquid–solid dynamics of ore-forming fluids, with the deposits having the same metal sources (Wang et al., 2020, 2021).

The Sichuan–Yunnan–Guizhou metallogenic province (SYGMP) includes several large Zn–Pb deposits (Huang et al., 2010; Zhou et al., 2018) and is an important source of Zn, Pb, Ag, Ge, and Cd (Liu et al., 2022; Luo et al., 2022; Zhou et al., 2022). Many studies of Cd isotopes in different Zn–Pb deposits have been undertaken there. The Maoping deposit has a homogeneous Pb–Zn–Cd isotopic composition (Wu et al., 2021), indicating that the metals were derived mainly from a binary source of mixed basement and carbonate rocks. The Jinding deposit has negative $\delta^{114/110}$Cd values (down to − 0.63 ‰; Li et al., 2019) reflecting the influence of bio-organisms during mineralization, with organic compounds enriched in heavy isotopes resulting in the enrichment of light isotopes in ore-forming fluids (Xie et al., 2017). Zn/Cd ratios and $\delta^{114/110}$Cd values of sedimentary (Zn/Cd = 13–367; $\delta^{114/110}$Cd = − 0.25 ‰ to + 0.82 ‰) and igneous (Emeishan basalts: Zn/Cd = 756–900; $\delta^{114/110}$Cd = − 0.13 ‰ to − 0.22 ‰) rocks in the Huize deposit are different. Based on this observation and published Cd isotopic data for the other seven Zn–Pb deposits in the SYG area, Zhu et al. (2021) proposed a two-fluid mixing model for the genesis of the eight large Zn − Pb deposits. Such studies indicate that deposits derived from sedimentary rocks have low Zn/Cd ratios and variable $\delta^{114/110}$Cd values, whereas those derived from mixtures of sedimentary and igneous rocks have higher Zn/Cd ratios and relatively small ranges of $\delta^{114/110}$Cd values. Cd isotopic compositions can thus be used to distinguish the contributions of different source beds.

The Zhugongtang deposit, NW Guizhou, is a newly discovered large-scale in the SYGMP with Pb + Zn reserves > 3.0 Mt. It is geochemically similar to the Huize deposit, as follows: (1) sphalerites of both deposits have similar S isotopic compositions (the Zhugongtang deposit, +14.3 ‰ to + 15.5 ‰, Liu et al., 2022; the Huize deposit, +12.5 ‰ to + 17.2 ‰, Li et al., 2006), and the S was likely derived from thermochemical sulfate reduction processes with the addition of organic matter (Li et al., 2006; Liu et al., 2022); (2) both deposits are rich in critical metals, as for example with Ge having reserves at 330 and 517 t, respectively (Wen et al., 2020); and (3) their Pb isotopic signatures indicate that their metal sources included mixtures of basement and sedimentary rocks (Han et al., 2007; Liu et al., 2022). However, the two deposits have different ore-hosting strata and mineralization ages: the Huize deposit is hosted mainly in the Baizuo Formation (C_1b; Han et al., 2007) and was formed in the late Permian (Huang et al., 2004), whereas the Zhugongtang deposit, which formed during the Late Triassic–Early Jurassic (Wei et al., 2021), is hosted mainly in the Qixia and Maokou formations (P_2q − m; Liu et al., 2022). Organic matter (e.g., bitumen) has been observed in country rocks of both deposits (Han et al., 2007; Wei et al., 2021). Although these deposits have similar geochemical characteristics, metal sources (especially for critical metals) have not been well constrained for the Zhugongtang deposit. In this study, Cd isotopic and major- and trace-element compositions of sulfides of different orebodies (Nos I-1 and IV-1) of the Zhugongtang deposit were determined to investigate the spatial distributions of Zn, Cd, and Fe to further constrain the metal sources of the deposit. The Cd isotopic signatures of Ge-rich and Ge-poor deposits in the SYGMP were compared to evaluate the relationships between Ge reserves and source beds.

2. Geological setting

The Yangtze Block lies in South China, bounded by the Songpan − Ganzi Orogenic Belt in the northwest, the Sanjiang Orogenic Belt in the southwest, and the Cathaysia Block in the southeast (Fig. 1A). It comprises mainly crystalline metamorphic series *meso*-Neoproterozoic folded basement (Qiu et al., 2000; Zhou et al., 2002, 2014a; Gao et al., 2011; Zhu et al., 2016; Zhou et al., 2018) and sedimentary cover of mainly Ediacaran to Lower–Middle Triassic shallow marine sedimentary strata (Zhang, 2008).

The SYGMP lies on the southwestern margin of the Yangtze Block, covering an area of > 170,000 km^2 (Zhou et al., 2001; Han et al., 2007) and surrounded by three regional fault belts: the NW-trending Kangdin–Yiliang–Shuicheng, N—S—trending Anninghe–Lvzhijiang, and NE-trending Mile–Shizong–Shuicheng fault belts (Fig. 1A). Strata in the SYGMP comprise basement and sedimentary rocks (Fig. 1B). Basement rocks are dominated by the lower Proterozoic Kangding, Dahongshan, and middle–upper Proterozioc Kunyang groups (Fig. 1B; Zhou et al., 2001; Huang et al., 2004; Zhu et al., 2021). The sedimentary sequence comprises predominantly Cambrian–late Permian marine and Late Triassic–Cenozoic continental sedimentary rocks (Fig. 1B; Yan et al., 2003; Zhou et al., 2013a; Hu et al., 2017). Permian Emeishan flood basalts are widely distributed over an area of > 250,000 km^2, covering the tringle area of Sichuan-Yunnan-Guizhou with thicknesses of several hundred meters to 5 km (Fig. 1B; Zhou et al., 2001). The SYGMP has undergone multiple tectonic events with the development of numerous NE − SW- and NW − SE-trending faults and folds (Fig. 1B; Zhou et al., 2018). >400 Zn–Pb deposits have been found in the SYGMP, accounting for 27 % of the total Zn–Pb reserves of China (Zhang et al., 2015). Most are hosted in the Ediacaran Dengying to Permian Qixia-Maokou formations (Liu and Lin, 1999; Huang et al., 2004).

The Zhugongtang Zn–Pb deposit, the largest discovered in the past decade, is in the southeastern part of the SYGMP, 15 km southwest of Hezhang County. In that mining area, the stratigraphic sequence comprises mainly early Silurian–late Permian sedimentary strata (Fig. 2; He et al., 2019). In ascending stratigraphic order, the exposed strata include the following: the upper Silurian Hanjiadian Formation, which comprises mainly sandstone and silty mudstone; the Lower Devonian Wangchengpo and Yaosuo formations that comprise mainly dolostone, siliceous dolostone, and limestone; the lower Carboniferous Xiangbai, Shangsi − Jiusi, and Baizuo formations, which are dominated by limestone, dolomitic limestone, and shale; the upper Carboniferous Huanglong and Maping formations, which are composed of limestone, bioclastic limestone, and dolostone; the lower Permian Liangshan Formation, which comprises mainly sandstone, calcareous shale, and argillaceous siltstone; the Permian Qixia and Maokou formations, which comprise mainly dolomitic and bioclastic limestones; the middle Permian Emeishan Formation, which comprises the Emeishan flood basalts and is unconformably underlain by the Maokou Formation; the upper Permian Longtan Formation, which comprises sandstone, shale, and claystone; and Quaternary cover (Fig. 2). The Qixia and Maokou formations are the principal ore-hosting strata of the Zhugongtang deposit (Liu et al., 2022). NW-, NE-, and E–W-trending fault systems are well developed in the area, with minor interlayer fractures (Fig. 2). Steep NW-trending faults (e.g., F1, F2, and F3) are the main ore-controlling and ore-hosting structures, whereas the NE- and E–W-trending faults generally formed after the ore and cut the NW-trending faults (Wu et al., 2019).

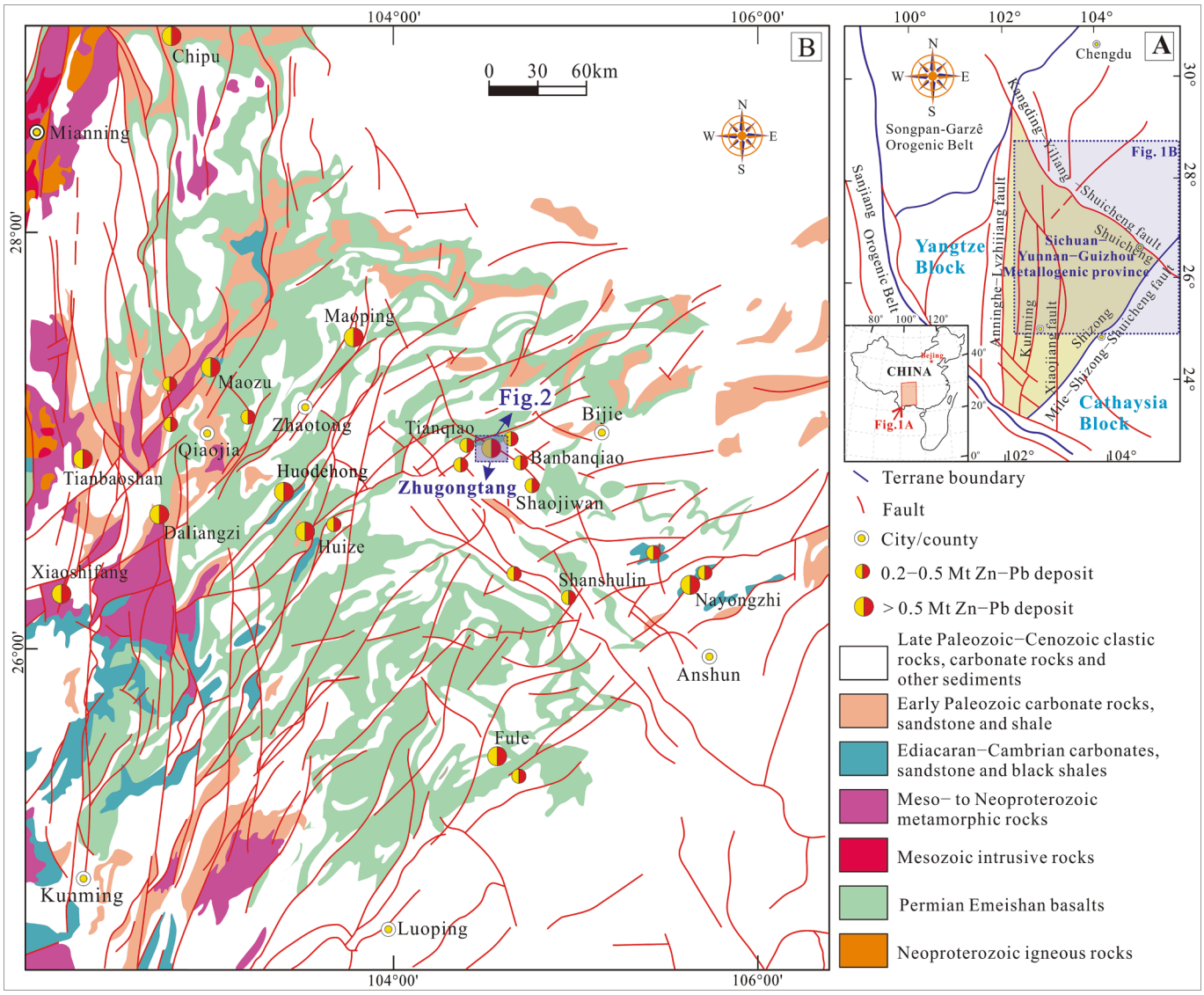

Fig. 1. (A) Simplified regional geological setting of the SYGMP on the SW margin of the Yangtze Block, S China. (B) Geological map of the SYGMP showing the distribution of regional structures, strata, Emeishan basalts, and the Zn–Pb deposits (modified from Liu and Lin, 1999; Zhou et al., 2018; Wei et al., 2021).

Orebodies are commonly stratiform, lenticular, and veined, and they occur along the F1, F2, and hidden (F20, F30) faults and interlayer fracture zones (He et al., 2019). The deposit includes 69 different-sized orebodies, which can be subdivided into 8 ore clusters (Nos I–VIII) based on their geological characteristics. Proven reserves of the Zhugongtang deposit are 3.27 Mt Zn + Pb ore at average grades of 6.76 % Zn and 2.27 % Pb, with trace amounts of Ge, Se, Cd, Cu, Ag, and Au (He et al., 2019). The No. I-1 orebody hosted within the F1 fault fracture zone is the largest, containing 65.96 % of total metal reserves with a length of 2300 m, width of 300 m, and thickness of < 1–65 m. It contains 0.44 Mt Pb and 1.38 Mt Zn ores with grades of 0.09–37.01 wt% Zn and 0.12–10.14 wt% Pb (He et al., 2019).

The ores comprise mainly sulfides with minor oxides (Wei et al., 2021; Fig. 3). Primary ore minerals are pyrite, sphalerite, and galena with minor tetrahedrite, limonite, gratonite, and cerussite. The main gangue minerals are calcite, dolomite, and rare quartz. Sulfide minerals have mainly euhedral–subhedral–anhedral granular, anhedral granular, metasomatic relict, inclusion, and cataclastic textures. Ore structures are dominated by massive, disseminated, veined, and banded structures. The Zn–Pb mineralization can be divided into three stages based on replacement relationships between sulfides: Stage I is the early ore stage comprising mainly coarse-grained euhedral pyrite and subhedral sphalerite with small amounts of irregular galena and quartz; Stage II is the main ore stage, with major ore minerals of coarse-grained sphalerite, galena, fine-grained pyrite, and minor K-feldspar, bitumen, and calcite; the late Stage III comprises mainly gangue minerals calcite and dolomite, with sparse galena occurring locally. Boundaries between orebodies and host rocks are clear, suggesting weak wall-rock alteration, and dolomitization and calcitization are closely associated with Zn–Pb mineralization.

3. Sampling and analysis

Representative sulfides were collected from mining tunnels ZGT-1–15 and drill-core ZK10405 (depth 721.6–423.3 m; Fig. 2). The former were crushed to 40–60 mesh and 20 sphalerite samples of different colors handpicked under a binocular microscope; these were then crushed to ~ 200 mesh. The latter samples were crushed directly to powder owing to their limited weight.

Samples of ~ 50 mg were weighed into Teflon digestion beakers for reaction with 3 mL concentrated HCl at 120 °C for > 24 h. After evaporation to dryness, residues were dissolved in 3 mL 2 % HNO_3 and

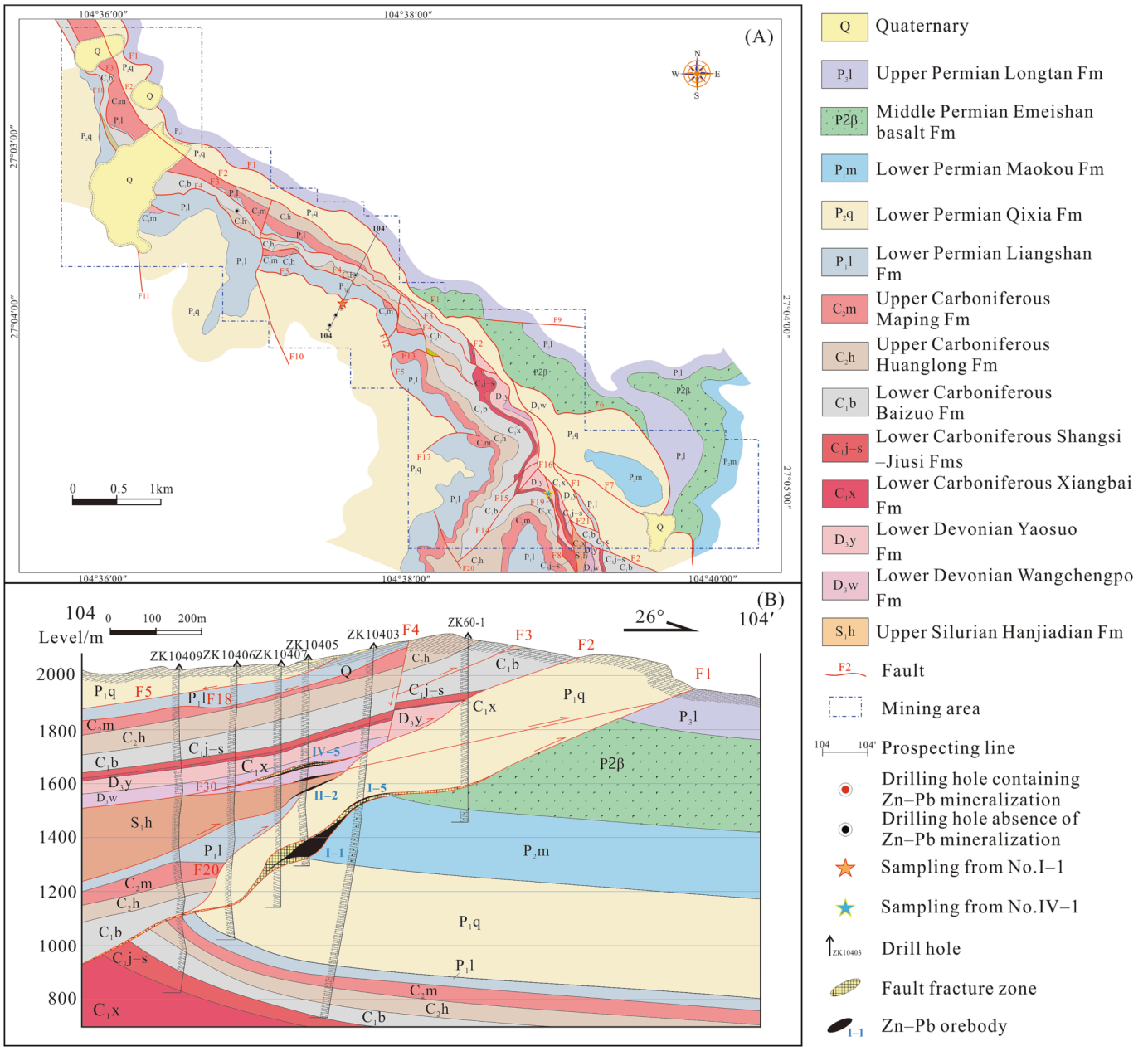

Fig. 2. (A) Geological map of the Zhugongtang Zn–Pb deposit showing the stratigraphy, structure, prospecting line, and sampling locations (modified from Wei et al., 2021). (B) Cross-section of the No. 104 – 104′ exploration line showing the stratigraphy, thrust system, drill-hole positions, and orebodies (modified from Wei et al., 2021).

centrifuged in 15 mL polypropylene centrifuge tubes at 4500 rpm for 10 mins. The supernatant was used for major- and trace-element (1 mL) and Cd isotope (1 mL) analyses following removal of interfering matrix elements such as Zn, Sn, In, and Pd from the latter following Zhu et al. (2013b).

Major- and trace-element compositions were determined by inductively coupled plasma–optical emission spectrometry (ICP–OES) at the ALS Laboratory Group, Guangzhou, China, using a method with the code ME–ICP02. Cadmium isotopic compositions of sulfides were determined by multicollector–ICP–mass spectrometry (MC–ICP–MS; Neptune Plus) at the State Key Laboratory of Ore Deposit Geochemistry, Institute of Geochemistry, Chinese Academy of Sciences, Guiyang, China. The standard–sample bracketing method coupled with a double spike was used for mass-bias correction, and the JMC reference material was used as a secondary Cd isotopic standard for quality control. Sample and standard solutions were diluted to 200 ng mL^{-1}, and the ^{111}Cd–^{110}Cd double-spike solution ($^{111}Cd/^{110}Cd \approx 2$) was added to achieve a total Cd sample/double-spike solution ratio of ~ 1. The Cd isotopic compositions of the double-spiked samples were computed by a MATLAB-based script with an iterative double-spike correction algorithm. The ^{114}Cd beam had an intensity of ~ 3 V for an uptake rate of ~ 50 μL min^{-1}. Details of instrumental parameters, measurement protocols, and the double-spike method are provided by Zhang et al. (2018) and Zhu et al. (2021).

Cadmium isotopic compositions are reported in per mil notation relative to the US National Institute of Standards and Technology (NIST) standard reference material (SRM) 3108Cd solution (Abouchami et al., 2013):$\delta^{114/110}Cd$ (‰) = $[(^{114}Cd/^{110}Cd)_{sample}/(^{114}Cd/^{110}Cd)_{NIST3108} - 1] \times 1000$

A duplicate sulfide standard (J-Zn-1, Japan) was added to monitor chemical purification and elemental and isotope analyses. The J-Zn-1was analyzed after each set of five samples. Long-term reproducibility of Cd isotopic data (±0.08 ‰) has been reported previously by Zhang

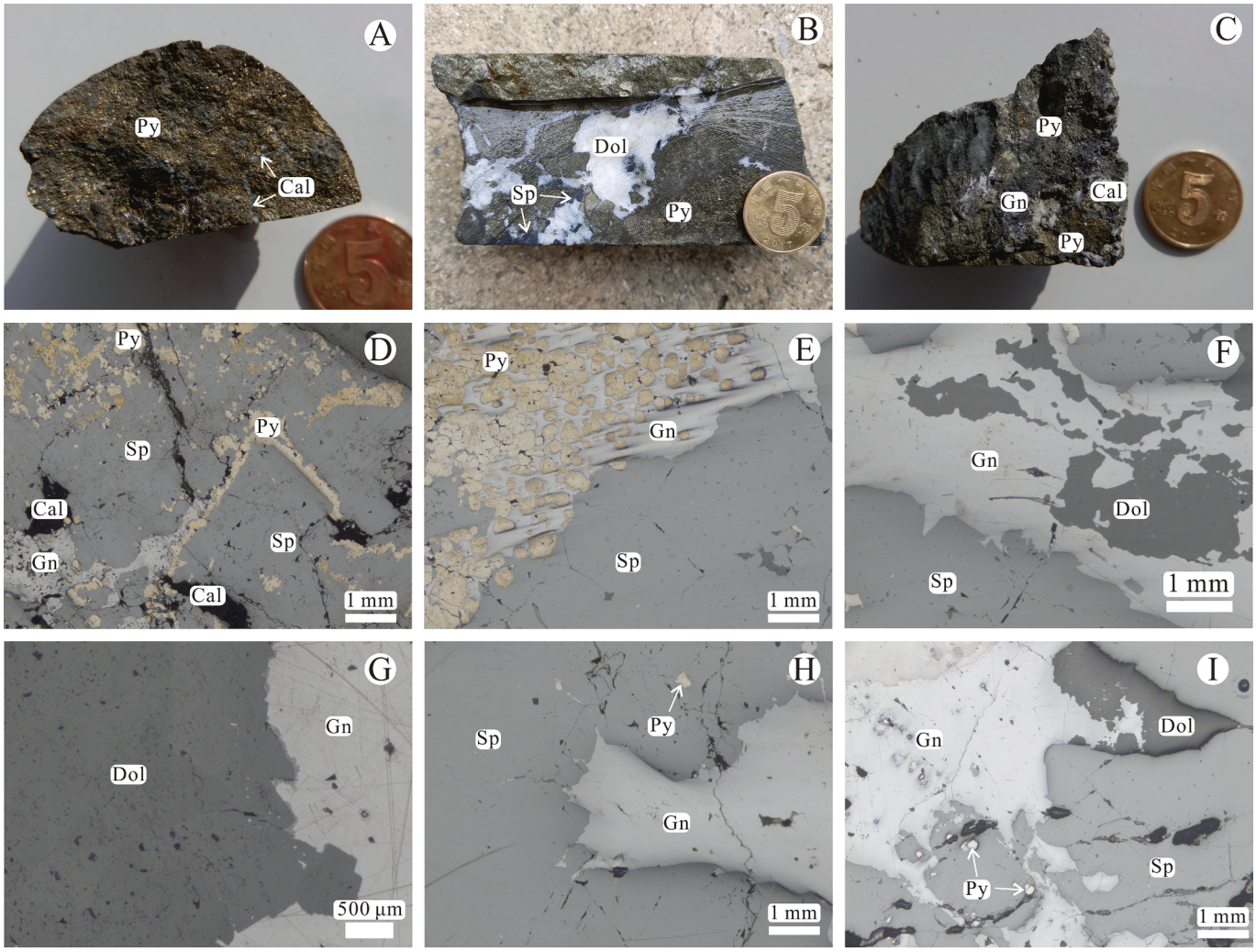

Fig. 3. Hand-specimen (A – C) and photomicrograph (D–E, all under reflected light) images of mineralization of the Zhugongtang deposit. (A) Hydrothermal calcite infilling the vug of massive pyrite; (B) breccia sulfide ore comprising massive pyrite, granular sphalerite, and dolomite; (C) massive pyrite overgrown with disseminated galena and calcite; (D) early fine – grain pyrite enclosed by sphalerite matrix, with pyrite and galena filling the sphalerite facture; (E) subhedral pyrite aggregates enclosed by galena replacing sphalerite; (F) galena – dolomite vein replaced in early sphalerite; (G) clear boundary between hydrothermal dolomite and galena; (H) galena replaced by sphalerite; (I) galena replacing cracked sphalerite, showing metasomatic relict texture. Abbreviations: Py = pyrite, Sp = sphalerite, Gn = galena, Cal = calcite; Dol = dolomite.

et al. (2016). The average JMC $\delta^{114/110}$Cd value was − 1.69 ‰ ± 0.08 ‰, consistent with literature values (−1.71 ‰ ± 0.06 ‰; Zhang et al., 2018). Duplicate analyses of J-Zn-1 yielded $\delta^{114/110}$Cd values of − 0.04 ‰ ± 0.03 ‰, −0.01 ‰ ± 0.03 ‰, and − 0.07 ‰ ± 0.06 ‰, consistent with published values (−0.05 ‰ ± 0.08 ‰; Yang et al., 2022a). Based on J-Zn-1 analyses, errors in Cd and Zn concentrations were < 5 % and 8 %, respectively.

4. Results

Cadmium isotopic compositions and Zn, Cd, and Fe contents are listed in Table 1. Due to sample impurity, Zn and Fe contents of drill-core samples were variable at 60–539501 μg g^{-1} (mean 111740 ± 324334 μg g^{-1}, 2SD; n = 34) and 7527–105889 μg g^{-1} (mean 43804 ± 52322 μg g^{-1}, 2SD; n = 34), respectively, and Cd contents were 10–938 μg g^{-1} (mean 319 ± 586 μg g^{-1}; 2SD; n = 19; 15 samples were below the detection limit). The hand-picked sphalerites from mining tunnels had much higher Zn, Cd, and Fe contents with mean values of 614723 ± 60030 μg g^{-1} (2SD; n = 20), 780 ± 476 μg g^{-1} (2SD; n = 20), and 9155 ± 24015 μg g^{-1} (2SD; n = 20), respectively.

Considering contamination by other minerals in sphalerite, Zn/Cd ratios were considered more suitable in reflecting variations in Cd content. Mean Zn/Cd ratios of drill-core and tunnel samples were 670 ± 295 (2SD; n = 19) and 848 ± 439 (2SD; n = 20), respectively.

Dill-core samples had minor Cd isotopic variations with $\delta^{114/110}$Cd values ranging from − 0.13 ‰ to + 0.06 ‰ (mean − 0.08 ‰ ± 0.08 ‰; 2SD; n = 14), whereas values for pure sphalerite were more variable at − 0.43 ‰ to − 0.03 ‰ (mean − 0.20 ‰ ± 0.08 ‰; 2SD; n = 20). Overall, the Zn/Cd ratios and Cd isotopic signatures of the Zhugongtang deposit samples were similar to those of the Huize deposit. Although the duplicate in-house standard (J-Zn-1) seemed to have variable $\delta^{114/110}$Cd values, they overlapped within the 2SD error range (Table 1).

5. Discussion

5.1. Geochemistry of sphalerite

Cadmium commonly occurs in sulfides by isomorphic substitution in other minerals, particularly with minor independent minerals such as CdS and $CdCO_3$ (Zhu et al., 2017; Yang et al., 2022a). It enters the sphalerite crystal lattice by direct substitution for Zn, with sphalerite thus being a significant Cd-bearing mineral (Cook et al., 2009).

Table 1
Cd isotopic compositions, major and trace elements concentrations for sulfides from the Zhugongtang deposit, China.

Sample No.	Depth (m) /Color	Cd (μg g^{-1})	Zn (μg g^{-1})	Fe (μg g^{-1})	Zn/Cd	$\delta^{114/110}Cd_{NIST-3108}$ (‰)	2SD
ZK10405 − 2	721.6	41	30,165	17,407	730	−0.13	0.08
ZK10405 − 4	718.5	/	470	51,727		/	/
ZK10405 − 5	717.7	/	378	68,487		/	/
ZK10405 − 6	715.8	/	313	79,133		/	/
ZK10405 − 7	713.9	/	744	63,457		/	/
ZK10405 − 8	712.2	54	31,848	101,413	586	−0.19	0.08
ZK10405 − 9	710.7	/	524	66,132		/	/
ZK10405 − 10	709.3	/	444	105,889		/	/
ZK10405 − 11	708.6	/	1593	85,872		/	/
ZK10405 − 12	707.4	/	93	50,932		/	/
ZK10405 − 13	705.0	370	155,391	21,987	420	−0.08	0.08
ZK10405 − 14	703.8	382	307,856	12,155	806	−0.08	0.08
ZK10405 − 15	700.4	/	60	59,820		/	/
ZK10405 − 17	697.6	/	1055	59,450		/	/
ZK10405 − 20	690.8	/	2192	56,566		/	/
ZK10405 − 22	686.2	10	6433	53,455	633	/	/
ZK10405 − 23	685.2	315	247,222	20,926	785	0.01	0.08
ZK10405 − 24	684.1	213	144,231	21,356	679	−0.22	0.08
ZK10405 − 25	684.6	738	539,501	35,135	731	0.04	0.08
ZK10405 − 26	682.0	622	308,091	18,465	495	/	/
ZK10405 − 27	680.9	938	452,096	19,960	482	0.06	0.08
ZK10405 − 28	677.6	30	25,000	46,774	827	0.01	0.08
ZK10405 − 29	680.9	611	304,481	14,002	498	−0.06	0.08
ZK10405 − 30	677.4	750	455,000	10,050	607	/	/
ZK10405 − 31	676.3	60	47,495	46,293	790	−0.07	0.08
ZK10405 − 32	673.0	/	1151	55,159		−0.09	0.08
ZK10405 − 33	672.1	313	205,184	7527	655	/	/
ZK10405 − 35	668.8	423	378,937	16,486	895	−0.23	0.08
ZK10405 − 36	669.6	/	823	60,823		−0.18	0.08
ZK10405 − 39	661.8	94	85,620	21,429	911	/	/
ZK10405 − 41–1	660.4	82	59,156	27,058	719	/	/
ZK10405 − 43	423.3	/	288	46,429		/	/
ZK10405 − 44	424.5	10	4861	37,624	491	/	/
ZK10405 − 45	434.7	/	450	29,959		/	/
ZGT − 1	yellow	551	594,172	869	1078	−0.07	0.08
ZGT − 1	red	573	631,770	988	1102	−0.19	0.08
ZGT − 2	yellow	1347	628,715	5531	467	−0.43	0.08
ZGT − 2	black	919	536,809	38,298	584	−0.14	0.08
ZGT − 3	yellow	575	627,333	897	1092	−0.39	0.08
ZGT − 3	black	589	559,340	3330	949	−0.27	0.08
ZGT − 3	red	561	631,615	1207	1126	−0.18	0.08
ZGT − 3	red	571	636,426	1386	1114	−0.21	0.08
ZGT − 4	yellow	625	629,829	873	1008	−0.22	0.08
ZGT − 5	yellow	632	637,133	1326	1009	−0.04	0.08
ZGT − 8	red	726	618,892	2791	853	−0.21	0.08
ZGT − 8	black	806	629,435	4155	781	−0.10	0.08
ZGT − 8	yellow	711	649,881	1948	914	−0.03	0.08
ZGT − 9	red	707	613,202	13,283	867	−0.12	0.08
ZGT − 9	yellow	755	630,581	4537	836	−0.39	0.08
ZGT − 10	black	1053	574,206	32,359	545	−0.07	0.08
ZGT − 13	red	968	630,587	11,882	652	−0.25	0.08
ZGT − 13	black	1313	596,641	29,572	454	−0.15	0.08
ZGT − 14	black	729	592,067	24,472	812	−0.18	0.08
ZGT − 15	yellow	898	645,832	3403	719	−0.40	0.08
J − Zn − 1–1		126	22,200	116,019	176	−0.04	0.03
J − Zn − 1–2		120	23,154	108,283	193	−0.01	0.03
J − Zn − 1–3		114	23,011	109,848	203	−0.07	0.06
Reference value		121[a]	2.22 ± 0.01[a, #]	11.8 ± 0.1[a, #]	*	−0.05[b]	0.08[b]

Note: [a]Okai et al. (2002); [b]Yang et al. (2022a); * = no reference value; / = below detection limit; [#] = Zn and Fe concentrations of J − Zn − 1 reported as %, the reference Cd content of J − Zn − 1 is from 114 to 121 ppm.

However, Cd may also be incorporated into sphalerite by substitution of (Fe^{2+}, Cd^{2+}) ↔ Zn^{2+}, as supported by the linear relationships between Fe and Cd or the Zn and Fe contents of sphalerites (Belissont et al., 2014). Owing to the impurity of sulfides in the drill-core samples, their Cd contents are not considered further here, although they exhibited a strong positive Zn–Cd correlation (R^2 = 0.89, Fig. 4A), suggesting sphalerite was the major Cd-bearing mineral. In pure sphalerites from the mining tunnels (orebody IV-1) there was no obvious Zn–Cd or Zn–Fe correlation (Table 1), but there was a strong Cd–Fe correlation, particularly in yellow sphalerite (R^2 = 0.76, Fig. 4B), implying that Cd occurs by direct (Fe^{2+}, Cd^{2+}) ↔ Zn^{2+} substitution rather than in sulfide (e.g., CdS) form.

5.2. Cadmium isotopic fractionation in sulfides

Sphalerites in most SYGMP deposits have a range of dark, red, and pale colors at hand specimen scale, and their formation sequence can be established on the basis of cross-cutting between colors. Dark sphalerites were formed earlier than the pale type, as shown by the former commonly being surrounded by the latter (Graeser, 1969; Zhu et al., 2017), as observed in the Huize (Zhu et al., 2021) and Tianqiao (Yang et al., 2022b) deposits. The different colored sphalerites thus provide a

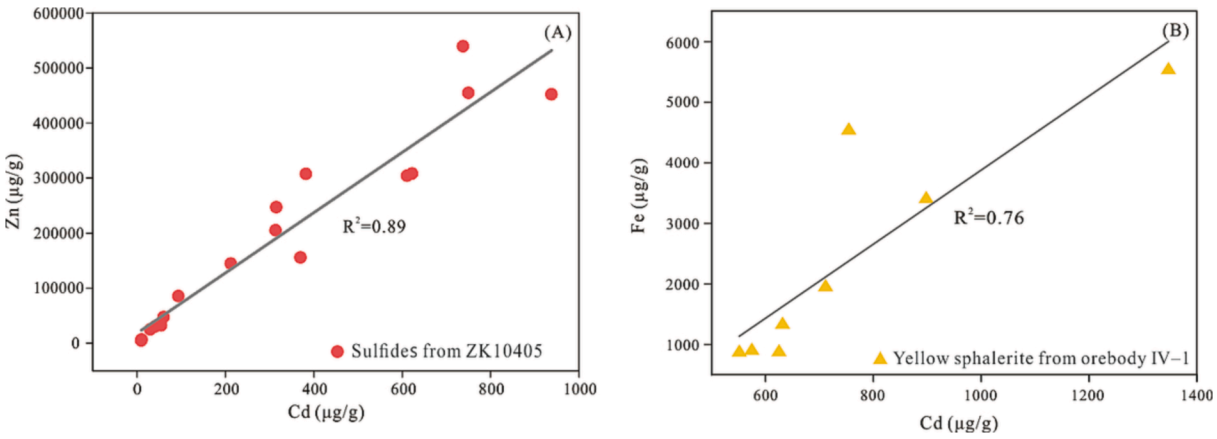

Fig. 4. Sulfide Zn–Cd and Fe–Cd diagrams. (A) Cd–Zn plot for drill-core ZK10405 (orebody I-1); (B) Cd–Fe plot for yellow sphalerites from mining tunnels (orebody IV-1).

precipitation sequence and record geochemical information pertaining to deposit formation. Cadmium isotopic fractionation in hydrothermal systems is generally dominated by mineral precipitation (Zhu et al., 2017), bacterial activity (Yang et al., 2022a), and fluid mixing (Zhu et al., 2021). Previous studies have shown that the lighter isotope is preferentially enriched in sulfides rather than fluids (Yang et al., 2015), with the earlier-formed dark sphalerites having lower $\delta^{114/110}$Cd values than the paler type. For example, for different colored sphalerites handpicked at hand-specimen scale from the Fule deposit, the $\delta^{114/110}$Cd values of dark sphalerites (−0.05 ‰ to + 0.35 ‰) were lower than those of pale sphalerites (+0.32 ‰ to + 0.59 ‰) (Zhu et al., 2017). The degree of Cd isotopic fractionation is closely related to ore-forming fluid temperatures during mineral precipitation (Yang et al., 2015). Based on previous studies of fluid inclusions in sphalerites, the main mineralization stage of the Zhugongtang deposit occurred at low temperatures of 105 °C–210°C (Liu et al., 2022). However, the degree of Cd isotopic fractionation caused by temperature is only 0.19 ‰ for $CdHS^+$ at 100 °C–200°C (Yang et al., 2015) lower than the observed fractionation of up to 0.49 ‰. Furthermore, some yellow sphalerites from tunnels of orebody IV-1 were more enriched in ^{110}Cd than the black or red sphalerites (Fig. 5), similar to the Huize deposit case but inconsistent with the Fule deposit. Mineral precipitation is thus unlikely to be the cause of Cd isotopic fractionation in sulfides of the Zhugongtang deposit, nor is the variation in $\delta^{114/110}$Cd values likely caused by bacterial activity, which may result in sulfides being strongly enriched in light Cd isotope, with $\delta^{114/110}$Cd values of down to − 0.74 ‰ (Yang et al., 2022a). The Cd and S isotopic compositions of sulfides do not indicate bacterial activity during formation of the Zhugongtang deposit, with $\delta^{114/110}$Cd and δ^{34}S values ranging from − 0.43 ‰ to + 0.06 ‰ and + 14.31 ‰ to + 15.53 ‰ (Liu et al., 2022), respectively.

Owing to the similarity of Cd isotopic signatures of the Huize and Zhugongtang deposits, we suggest that Cd isotopic variations in the Zhugongtang deposit are caused mainly by mixing of fluids from different sources.

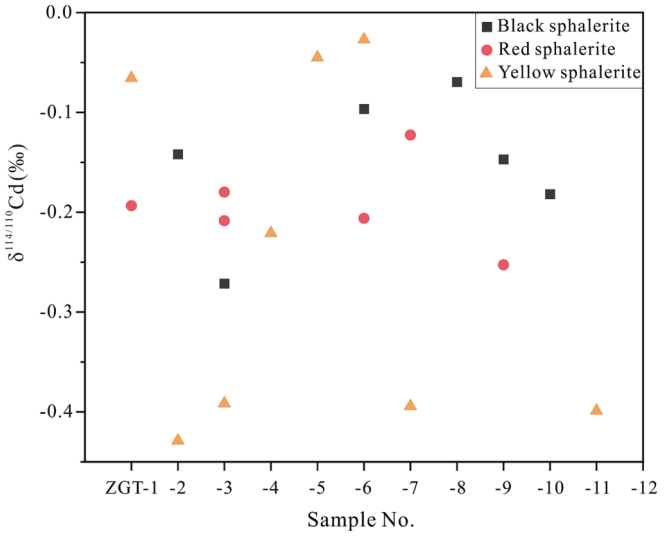

Fig. 5. Comparison of Cd isotopic compositions of different-colored sphalerites from mining tunnels (orebody IV-1).

5.3. Metal sources of the Zhugongtang deposit

Owing to similarities in geochemical behavior between Zn and Cd in hydrothermal systems, Cd isotopic compositions are commonly considered alongside Zn/Cd ratios in constraining metal sources in such systems.

We used a dataset of igneous (basic − intermediate − acidic) reference materials including BCR-2, BIR-1, BHVO-2, W-2, AGV-2, and GSP-2 with $\delta^{114/110}$Cd values of − 0.21 ‰ to + 0.15 ‰ tending to zero, and high Zn/Cd ratios of 515–1319 (Table S2; Gladney and Roelandts, 1988; Chen et al., 2016; Wiggenhauser et al., 2016; Palk et al., 2018; Braukmüller et al., 2020; Liu et al., 2020a; Tan et al., 2020; Zhu et al., 2021). Cadmium isotopic compositions of carbonates from the Ediacaran Xiaofenghe section of the Yangtze Platform, South China, also exhibit significant variations ($\delta^{114/110}$Cd = − 0.68 ‰ to 0.21 ‰; Hohl et al., 2017; Table S3), indicating the highly variable $\delta^{114/110}$Cd values of sedimentary rocks relative to those of igneous rocks.

The Zn/Cd ratios of the studied sphalerites from the Zhugongtang deposit ranged from 420 to 1126. Most samples were enriched in light Cd isotope, with $\delta^{114/110}$Cd values of − 0.43 ‰ to + 0.06 ‰. Compared with sedimentary rocks and Emeishan basalts from the Huize deposit, and igneous rock reference materials, we found that the observed Zn/Cd ratios and $\delta^{114/110}$Cd values of sulfides from the deposit are between sedimentary and igneous rocks. However, the Cd isotopic compositions of most samples varied within the ranges of sedimentary and igneous rocks, with a few samples being slightly enriched in light Cd isotopes. A mixing model involving ore-forming fluids derived from sedimentary and igneous rocks would thus likely account for the Cd isotopic variation of the Zhugongtang deposit.

To better assess the contributions of two sources, it was necessary to obtain their average Zn and Cd contents and $\delta^{114/110}$Cd values. The Zn and Cd contents of peripheral strata from the Ediacaran Dengying Formation (Z_2d) to the Permian Liangshan Formation (P_1 l) of the Huize deposit are highly variable with values of 2.4–62.9 and 0.04–0.66 μg

g^{-1}, respectively (Huang et al., 2004). Therefore, we chose basalt and carbonate rock from eastern China as the two endmembers for which Zn and Cd contents have been published (Yan and Chi, 1997) as $Zn_{basalts}$ = 120 μg g^{-1}, $Cd_{basalts}$ = 0.10 μg g^{-1}, $Zn_{carbonate\ rocks}$ = 18 μg g^{-1}, and $Cd_{carbonate\ rocks}$ = 0.13 μg g^{-1}. For $\delta^{114/110}$Cd values, we adopted the Cd isotopic composition of sedimentary rocks from the Huize ore district and the Xiaofenghe section (−0.68 ‰ to + 0.82 ‰; Zhu et al., 2017, 2021) and bulk silicate Earth (−0.06 ‰; Pickard et al., 2022). In the mixing model, the basalt is comparable to the Proterozoic basement, which comprises mainly igneous rock, whereas sedimentary rocks of the Huize ore district and the Xiaofenghe section are similar to country rocks of the Zhugongtang deposit due to their spatial distribution within the SYGMP (Figs. 1 and 6).

Based on mass balance, we calculated $\delta^{114/110}$Cd values and Zn/Cd ratios for endmember mixtures of given proportions (Fig. 6; Table S4) and considered these alongside the Zn/Cd ratios and Cd isotopic compositions of sulfides from 11 typical Zn − Pb deposits of the SYGMP. As shown in Fig. 6, the metal sources of deposits in the SYGMP can be divided into groups I and II. The Group I metal source was derived mainly from sedimentary rocks (e.g., the Daliangzi and Jinshachang deposits) and that of Group II from basement (e.g., the Huize and Zhugongtang deposits). This classification is consistent with previous studies; for example, Zhou et al. (2015) investigated the Pb isotopic ratios of sulfides and sedimentary rocks of the Jinshachang deposit and suggested that Pb was derived from Cambrian sedimentary rocks.

The strong negative correlation observed between mean $\delta^{114/110}$Cd and 1/Cd values (R^2 = 0.81, Fig. 7) of sulfides of the 11 typical Zn–Pb deposits suggests that the mixing model is applicable to the Zhugongtang deposit, consistent with earlier in situ Pb isotopic ratios (Wei et al., 2021).

The Ge grades of sphalerites and reserves of the 11 Zn − Pb deposits indicate that the deposits can be subdivided into two types based on sphalerite Ge contents: "Ge-poor" (Ge contents < 100 μg g^{-1}) and "Ge-rich" deposits (Ge > 100 μg g^{-1}). The Ge-rich deposits (Huize, Nayongzh, and Zhugongtang) had low $\delta^{114/110}$Cd values (mean − 0.07 ‰), similar to those of igneous rocks. Ge-poor deposits, excluding the Fule deposit, had similar Zn/Cd ratios and $\delta^{114/110}$Cd values to those of sedimentary rocks, implying that sediments contributed limited Ge to those deposits, where Ge was derived mainly from igneous basement rocks rather than sedimentary rocks, and the Ge contribution of

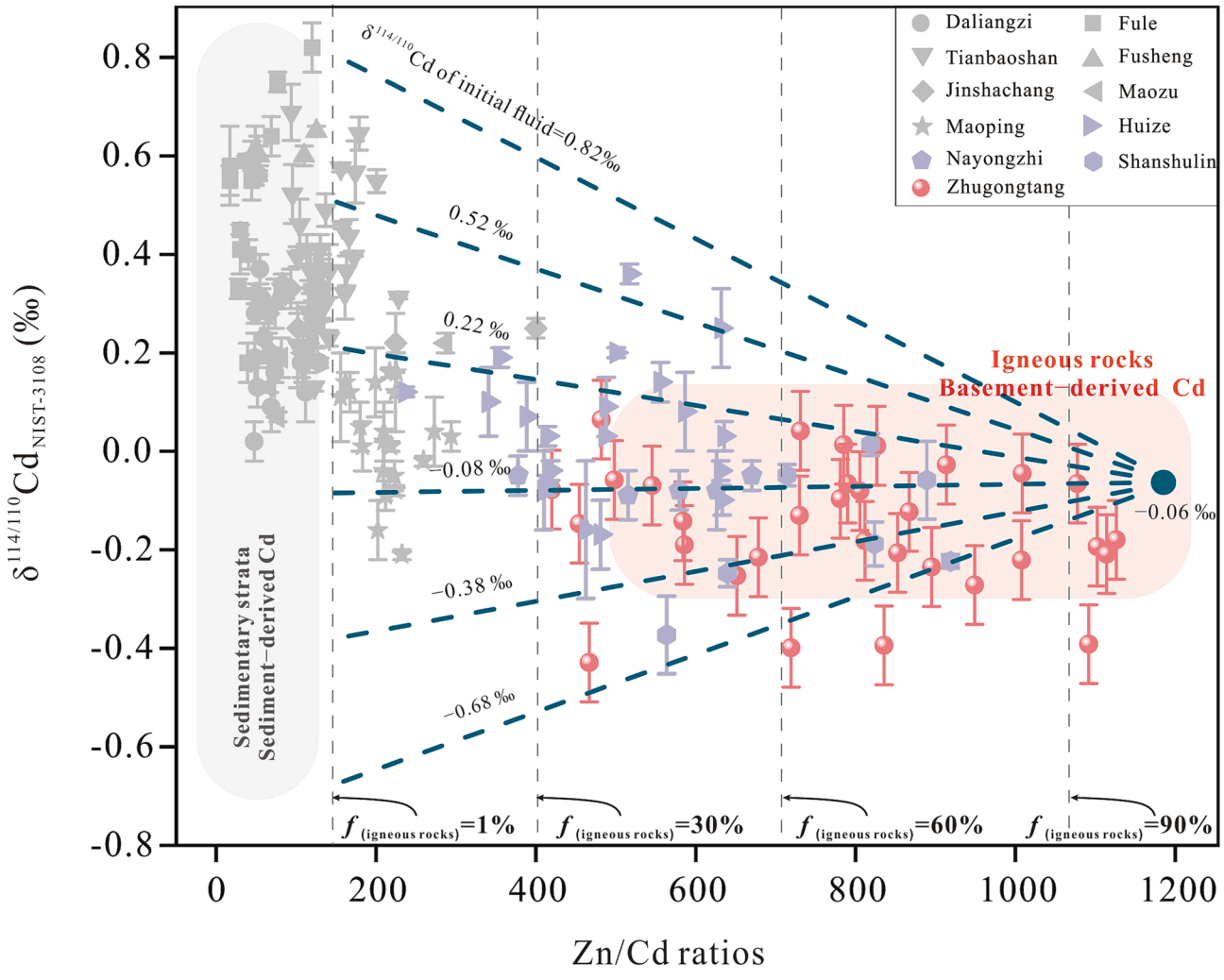

Fig. 6. (Zn/Cd)–Cd isotopic composition plot for sphalerite from 11 SYGMP Zn–Pb deposits. Gray and pink areas represent ranges of $\delta^{114/110}$Cd values and Zn/Cd ratios for sedimentary and igneous rocks, respectively. Crosses represent mixing results of sedimentary and igneous rocks with various mixing proportion (f) and Cd isotopic compositions of initial fluid ($\delta^{114/110}$Cd). Data sources (Tables S1–S3): Daliangzi, Fusheng, Jinshachang, and Maozu (Xu et al., 2020); Fule (Zhu et al., 2017); Tianbaoshan (Zhu et al., 2016; Xu et al., 2020); Shanshulin and Huize (Zhu et al., 2021); Nayongzhi (Song et al., 2022); Maoping (Wu et al., 2021); sedimentary rocks (Zhu et al., 2017, 2021); bulk silicate Earth (Pickard et al., 2022); Emeishan basalts (Zhu et al., 2021); igneous rock reference materials (Cd contents and $\delta^{114/110}$Cd values, Zhu et al., 2021; Liu et al., 2020a; Tan et al., 2020; Wiggenhauser et al., 2016; Palk et al., 2018; Zn contents, Chen et al., 2016; Gladney and Roelandts, 1988; Braukmüller et al., 2020), Zn and Cd contents of basalt and carbonate rock of eastern China (Yan and Chi, 1997).

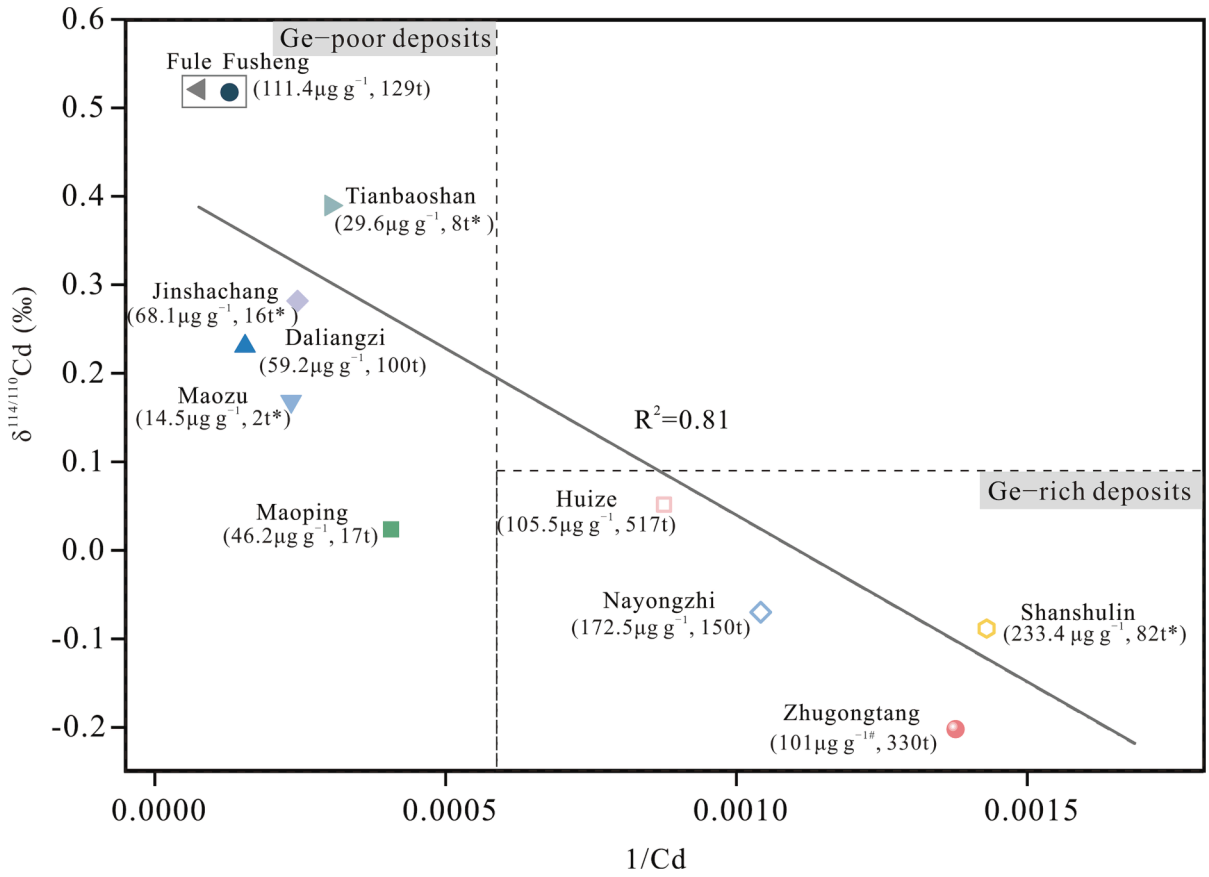

Fig. 7. Mean (1/Cd)–$\delta^{114/110}$Cd diagram for sphalerites from 11 SYGMP Zn–Pb deposits showing average Ge contents and reserves in parentheses. Data sources: average Ge contents of Jinshachang (Wu, 2013), Daliangzi (Li et al., 2022), Fule (Liu et al., 2020b), Maozu (Li et al., 2020), Maoping (Ye et al., 2019), Tianbaoshan (Ye et al., 2016), Huize (Meng, 2014), Shanshulin (Yang et al., 2022b), and Nayongzhi (Wei et al., 2018) deposits; Ge reserves of the Huize, Nayongzhi, and Zhugongtang (Wen et al., 2020), Fule and Maoping (Ye et al., 2019), Daliangzi (Li et al., 2022), Jinshachang (Zhou et al., 2015), Maozu (Li et al., 2020), Tianbaoshan (Zhou et al., 2013b), Shanshulin (Zhou et al., 2014b), and Zhugongtang (Wen et al., 2020; He et al., 2019) deposits, with other data sources as listed in Fig. 6. Note: The Fule and Fusheng deposits are in different counties, but their orebodies are connected underground. The regression line represents the linear relationship between the mean 1/Cd and $\delta^{114/110}$Cd values of sphalerites (R^2 = 0.81), excluding samples from a drill-core from the Zhugongtang deposit (Tables S1 and S5). * indicates estimated Ge reserves based on Ge contents and Zn reserves; # indicates the estimated Ge grade of the Zhugongtang deposit based on Ge and Zn + Pb reserves.

basement likely determined whether the deposit was Ge-rich or -poor. This is supported by the lower Ge content of carbonates (0.09 μg g^{-1}) and the relatively high contents of igneous rocks (e.g., mafic rocks, 1.4 μg g^{-1}; Bernstein, 1985). It has been suggested that the Ge in Ge-rich coal was derived from igneous rocks (e.g., the Lincang and Wulantuga coal deposits; Qi et al., 2011; Dai et al., 2015), further indicating the close relationship between Ge-rich deposits and igneous rocks.

6. Conclusion

The Cd isotopic compositions and major- and trace-element contents of sulfides from mining tunnels (orebody IV-1) and a drill-core (orebody I-1) of the Zhugongtang deposit were investigated. Drill-core samples had low purity but exhibited a strong positive correlation (R^2 = 0.89) between Zn and Cd contents, suggesting sphalerite is the main Cd-bearing mineral. The Cd contents of pure sphalerite were positively correlated with Fe contents in tunnel samples, especially in yellow sphalerite (R^2 = 0.76). Cadmium was thus likely incorporated into sphalerites via (Fe^{2+}, Cd^{2+}) ↔ Zn^{2+} substitution.

All samples were relatively enriched in ^{110}Cd ($\delta^{114/110}$Cd = − 0.43 ‰ to + 0.06 ‰), with variable Zn/Cd ratios of 420–1126. The different Cd isotopic signatures and Zn/Cd ratios of sedimentary and igneous rocks in the study area support a mixing model for the metal sources of the deposit. Cadmium contents and isotopic compositions of sphalerite from 11 typical Zn–Pb deposits in the SYGMP indicate a strong negative correlation between $\delta^{114/110}$Cd and 1/Cd values, suggesting these deposits have different metal sources. Based on the contributions of basement and sediments, these deposits can be divided into groups I and II, with the former being derived mainly from sedimentary rocks as Ge-poor deposits (excluding the Fule deposit) and the latter from basement as Ge-rich deposits. Owing to the low Ge contents of carbonates (0.09 μg g^{-1}), the predominant type of sediment in the SYGMP, and the higher Ge contents of the abundant basement igneous rocks (mafic rocks, 1.4 μg g^{-1}), we conclude that igneous rocks are the parental source of Ge in these deposits, as supported by Ge in Ge-rich coal deposits being derived mainly from igneous rocks.

Declaration of Competing Interest

The authors declare that they have no known competing financial interests or personal relationships that could have appeared to influence the work reported in this paper.

Data availability

Data will be made available on request.

Acknowledgments

This research was financially supported by the Technology Foundation of Guizhou Province (Grant [2019]1459), the National Natural Science Foundation of China (Grants 92162214, 41773015, U1812402, and 92162218), the Key Research and Development Program of Yunnan Province (Grant 202103AQ100003), and a special fund managed by the State Key Laboratory of Ore Deposit Geochemistry, Chinese Academy of Sciences.

Appendix A. Supplementary data

Supplementary data to this article can be found online at https://doi.org/10.1016/j.oregeorev.2023.105426.

References

Abouchami, W., Galer, S.J.G., Horner, T.J., Rehkämper, M., Wombacher, F., Xue, Z.C., Lambelet, M., Gault-Ringold, M., Stirling, C.H., Schönbächler, M., Shiel, A.E., Weis, D., Holdship, P.F., 2013. A common reference material for cadmium isotope studies—NIST SRM 3108. Geostand. Geoanal. Res. 37 (1), 5–17.

An, Y.J., Huang, F., 2014. A review of Mg isotope analytical methods by MC–ICP–MS. J. Earth Sci. 25 (5), 822–840.

Anbar, A.D., Rouxel, O., 2007. Metal Stable Isotopes in Paleoceanography. Annu. Rev. Earth Planet. Sci. 35, 717–746.

Belissont, R., Boiron, M.C., Luais, B., Cathelineau, M., 2014. LA–ICP–MS analyses of minor and trace elements and bulk Ge isotopes in zoned Ge–rich sphalerites from the Noailhac–Saint–Salvy deposit (France): insights on incorporation mechanisms and ore deposition processes. Geochim. Cosmochim. Acta 126, 518–540.

Bernstein, L.R., 1985. Germanium geochemistry and mineralogy. Geochim. Cosmochim. Acta 49 (11), 2409–2422.

Blum, J.D., Johnson, M.W., 2017. Recent Developments in Mercury Stable Isotope Analysis. Rev. Mineral. Geochem. 82 (1), 733–757.

Braukmüller, N., Wombacher, F., Bragagni, A., Münker, C., 2020. Determination of Cu, Zn, Ga, Ag, Cd, In, Sn and Tl in geological reference materials and chondrites by isotope dilution ICP–MS. Geostand. Geoanal. Res. 44 (4), 733–752.

Cai, M.H., Peng, Z., Hu, Z.S., Li, Y., 2020. Zn, He–Ar and Sr–Nd isotopic compositions of the Tongkeng Tin–polymetallic ore deposit in south China: Implication for ore genesis. Ore Geol. Rev. 124, 103605.

Chen, S., Liu, Y.C., Hu, J.Y., Zhang, Z.F., Hou, Z.H., Huang, F., Yu, H.M., 2016. Zinc isotopic compositions of NIST SRM 683 and whole–rock reference materials. Geostand. Geoanal. Res. 40 (3), 417–432.

Cook, N.J., Ciobanu, C.L., Pring, A., Skinner, W., Shimizu, M., Danyushevsky, L., SainiEidukat, B., Melcher, F., 2009. Trace and minor elements in sphalerite: A LA–ICPMS study. Geochim. Cosmochim. Acta 73 (16), 4761–4791.

Craddock, P.R., Dauphas, N., 2011. Iron isotopic compositions of geological reference materials and chondrites. Geostand. Geoanal. Res. 35, 101–123.

Dai, S.F., Liu, J.J., Ward, C.R., Hower, J.C., Xie, P.P., Jiang, Y.F., Hood, M.M., O'Keefe, J. M.K., Song, H., 2015. Petrological, geochemical, and mineralogical compositions of the low–Ge coals from the Shengli Coalfield, China: A comparative study with Ge–rich coals and a formation model for coal–hosted Ge ore deposit. Ore Geol. Rev. 71, 318–349.

Fan, H.F., Wen, H.J., Hu, R.Z., Zhang, Y.X., 2007. Stable isotope of redox–sensitive elements (Se, Cr, Mo). Earth Sci. Front. 14 (5), 264–276. In Chinese with English abstract.

Gao, S., Yang, J., Zhou, L., Li, M., Hu, Z.C., Guo, J.L., Yuan, H.L., Gong, H.J., Xiao, G.Q., Wei, J.Q., 2011. Age and growth of the Archean Kongling terrain, South China, with emphasis on 3.3 Ga granitoid gneisses. Am. J. Sci. 311, 153–182.

Gladney, E.S., Roelandts, I., 1988. 1987 compilation of elemental concentration data for USGS BIR–1, DNC–1 and W–2. Geostand. Newsl. 12 (1), 63–118.

Graeser, S., 1969. Minor elements in sphalerite and galena from Binnatal. Contrib. Mineral. Petrol. 24, 156–163.

Han, R.S., Liu, C.Q., Huang, Z.L., Chen, J., Ma, D.Y., Lei, L., Ma, G.S., 2007. Geological features and origin of the Huize carbonate–hosted Zn–Pb–(Ag) district, Yunnan. South China. Ore Geol. Rev. 31, 360–383.

He, L.L., Wu, D.W., Zhao, F., Jin, X.L., Bai, G.H., Chen, Z.X., Wang, J., Huang, Q., Cai, J. C., 2019. Geological characteristics, exploration model and prospecting direction of the Zhugongtang Ultra–large Pb–Zn deposit in Guizhou Province. Guizhou Geol. 26, 101–109 in Chinese with English abstract.

Hohl, S.V., Galer, S.J.G., Gamper, A., Becker, H., 2017. Cadmium isotope variations in Neoproterozoic carbonates – A tracer of biologic production? Geochem. Perspect. Lett. 3 (1), 32–44.

Hu, R., Fu, S., Huang, Y., Zhou, M., Fu, S., Zhao, C., Wang, Y., Bi, X., Xiao, J., 2017. The giant South China Mesozoic low–temperature metallogenic domain: Reviews and a new geodynamic model. J. Asian Earth Sci. 137, 9–34.

Huang, Z.L., Chen, J., Han, R.S., Li, W.B., Liu, C.Q., Zhang, Z.L., Ma, D.Y., Gao, D.R., Yang, H.L., 2004. Geochemistry and Ore–formation of the Huize Giant Lead-Zinc Deposit, Yunnan Province, China: Discussion on the Relationship between Emeishan Flood Basalts and Lead-Zinc Mineralization. Geological Publishing House, Beijing (in Chinese).

Huang, Z.L., Li, X.B., Zhou, M.F., Li, W.B., Jin, Z.G., 2010. REE and C–O isotopic geochemistry of calcites from the word–class Huize Pb–Zn deposits, Yunnan, China: implication for the ore genesis. Acta Geol. Sin. (Engl. Ed.) 84, 597–613.

Lehmann, B., Pašava, J., Šebek, O., Andronikov, A., Frei, R., Xu, L., Mao, J.W., 2022. Early Cambrian highly metalliferous black shale in South China: Cu and Zn isotopes and a short review of other non-traditional stable isotopes. Miner. Deposita. 57, 1167–1187.

Leybourne, M.I., Peter, J.M., Kidder, J.A., Layton-Matthews, D., Petrus, J.A., Rissmann, C.F.W., Voinot, A., Bowell, R., Kyser, T.K., 2022. Stable and Radiogenic Isotopes in the Exploration for Volcanogenic Massive Sulfide Deposits. Canad. Mineral. 60 (3), 433–468.

Li, L.J., Han, R.S., Zhang, Y., Wu, J.B., Feng, Z.X., 2022. Trace element signatures of sphalerite in the Sichuan Daliangzi Ge−rich Pb−Zn deposit and its implications for deep ore prospecting. Front. Earth Sci. 10, 928738.

Li, W.B., Huang, Z.L., Zhang, G., 2006. Sources of the ore metals of the Huize ore field in Yunnan province: constraints from Pb, S, C, H, O and Sr isotope geochemistry. Acta Petrol. Sin. 22 (10), 2567–2580. In Chinese with English abstract.

Li, M.L., Liu, S.A., Xue, C.J., Li, D.D., 2019. Zinc, cadmium and sulfur isotope fractionation in a supergiant MVT deposit with bacteria. Geochim. Cosmochim. Acta 265, 1–18.

Li, Z.L., Ye, L., Hu, Y.S., Wei, C., Huang, Z.L., Yang, Y.L., Danyushevsky, L., 2020. Trace elements in sulfides from the Maozu Pb–Zn deposit, Yunnan Province, China: Implications for trace–element incorporation mechanisms and ore genesis. Am. Mineral. 105, 1734–1751.

Liu, Y., He, L.L., Yang, K.G., Ali, P., Zhou, Q., Wu, P., Wu, D.W., Wang, J., Cai, J.C., 2022. Constraints of C−H−O−S−Pb isotopes and fluid inclusions on the origin of the giant Zhugongtang carbonate–hosted Pb–Zn deposit in South China. Ore Geol. Rev. 151, 105192.

Liu, S.A., Huang, J., Liu, J.G., Wörner, G., Yang, W., Tang, Y.J., Chen, Y., Tang, L.M., Zheng, J.P., Li, S.G., 2015. Copper isotopic composition of the silicate Earth. Earth Planet. Sci. Lett. 427, 95–103.

Liu, H.C., Lin, W.D., 1999. Regularity research of Ag. Zn. Pb ore deposits northeast Yunnan Province. Yunnan University Press, Kunming, 1–468 (in Chinese).

Liu, M.S., Zhang, Q., Zhang, Y.N., Zhang, Z.F., Huang, F., Yu, H.M., 2020a. High–precision Cd isotope measurements of soil and rock reference materials by MC–ICP–MS with double spike correction. Geostand. Geoanal. Res. 44 (1), 169–182.

Liu, T.T., Zhu, C.W., Yang, G.S., Zhang, G.S., Fan, H.F., Zhang, Y.X., Wen, H.J., 2020b. Primary study of germanium isotope composition in sphalerite from the Fule Pb–Zn deposit, Yunnan province. Ore Geol. Rev. 120, 103466.

Lu, D.W., Zhang, T.Y., Yang, X.Z., Su, P., Liu, Q., Jiang, G.B., 2017. Recent advances in the analysis of non–traditional stable isotopes by multi–collector inductively coupled plasma mass spectrometry. J. Analyt. Atomic Spectrom. 32, 1848–1861.

Luo, K., Cugerone, A., Zhou, M.F., Zhou, J.X., Sun, G.T., Xu, J., He, K.J., Lu, M.D., 2022. Germanium enrichment in sphalerite with acicular and euhedral textures: an example from the Zhulingou carbonate–hosted Zn(–Ge) deposit, South China. Miner. Deposita 57, 1343–1365.

Meng, Y.M., 2014. Application of Ge isotopes to mineral deposits: Examples from the Wulantuga Ge deposit of Inner Mongolia, the Huize and other Pb–Zn deposits of SW China. A dissertation submitted to Chinese Academy of Science for a doctor degree, Guiyang (In Chinese with English abstract).

Millet, M.A., Dauphas, N., 2014. Ultra–precise titanium stable isotope measurements by double–spike high resolution MC–ICP–MS. J. Anal. At. Spectrom. 29, 1444–1458.

Mondillo, N., Wilkinson, J.J., Boni, M., Weiss, D.J., Mathur, R., 2018. A global assessment of Zn isotope fractionation in secondary Zn minerals from sulfide and non–sulfide ore deposits and model for fractionation control. Chem. Geol. 500, 182–193.

Okai, T., Terashima, S., Imai, N., 2002. Collaborative analysis of GSJ geochemical reference materials JCu–1 (Copper ore) and JZn–1 (Zinc ore). Bunseki Kagaku 51 (10), 973–977.

Palk, E., Andreasen, R., Rehkämper, M., Stunt, A., Kreissig, K., Coles, B., Schönbächler, M., Smith, C., 2018. Variable Tl, Pb, and Cd concentrations and isotope compositions of enstatite and ordinary chondrites—Evidence for volatile element mobilization and decay of extinct ^{205}Pb. Meteorit. Planet. Sci. 53 (2), 167–186.

Pickard, H., Palk, E., Schönbächler, M., Moore, R.E.T., Coles, B.J., Kreissig, K., Nilsson-Kerr, K., Hammond, S.J., Takazawa, E., Hémond, C., Tropper, P., Barfod, D.N., Rehkämper, M., 2022. The cadmium and zinc isotope compositions of the silicate Earth – implications for terrestrial volatile accretion. Geochim. Cosmochim. Acta 338 (1), 165–180.

Prytulak, J., Nielsen, S., Ionov, D., Halliday, A., Harvey, J., Kelley, k., Niu, Y., Peate, D., Shimizu, K., Sims, K., 2013. The stable vanadium isotope composition of the mantle and mafic lavas. Earth Planet. Sci. Lett. 365, 177–189.

Qi, H.W., Rouxel, O., Hu, R.Z., Bi, X.W., Wen, H.J., 2011. Germanium isotopic systematics in Ge–rich coal from the Lincang Ge deposit, Yunnan, Southwestern China. Chem. Geol. 286 (3–4), 252–265.

Qiu, Y.M., Gao, S., McNaughton, N.J., Groves, D.I., Ling, W.L., 2000. First evidence of >3.2 Ga continental crust in the Yangtze craton of south China and its implications for Archean crustal evolution and Phanerozoic tectonics. Geology 28, 11–14.

Song, W.R., Zhu, C.W., Yang, Z., Wu, Y.Z., Li, Q.K., Gao, L.S., Zhang, J.W., Zhang, Y.X., Fan, H.F., Wen, H.J., 2022. Genesis of the Nayongzhi Lead–zinc Deposit in Guizhou Province: Constraints From Cd Isotopes and Trace Elements. Bull. Mineral. Petrol. Geochem. 41 https://doi.org/10.19658/j.issn.1007-2802.2022.41.072 (In Chinese with English abstract).

Spry, P.G., Mathur, R.D., Teale, G.S., Godfrey, L.V., 2022. Zinc, sulfur and cadmium isotopes and Zn/Cd ratios as indicators of the origin of the supergiant Broken Hill

Pb–Zn–Ag deposit and other Broken Hill–type deposits, New South Wales. Australia. Geol. Mag. 159 (10), 1787–1808.
Tan, D.C., Zhu, J.M., Wang, X.L., Han, G.L., Lu, Z., Xu, W.P., 2020. High–sensitivity determination of Cd isotopes in low–Cd geological samples by double spike MC–ICP–MS. J. Anal. At. Spectrom. 35 (4), 713–727.
Teng, F.Z., Dauphas, N., Watkins, J.M., 2017. Non-Traditional Stable Isotopes: Retrospective and Prospective. Rev. Mineral. Geochem. 82 (1), 1–26.
Wang, D., Zheng, Y.Y., Mathur, R., Yu, M., 2020. Fractionation of cadmium isotope caused by vapour–liquid partitioning in hydrothermal ore–forming system: A case study of the Zhaxikang Sb–Pb–Zn–Ag deposit in Southern Tibet. Ore Geol. Rev. 119, 103400.
Wang, D., Zheng, Y.Y., Mathur, R., Qiu, K.F., Wu, H.J., Ren, H., Wang, E.R., Li, Y.J., Yi, J. Z., 2021. Zinc and cadmium isotopic constraints on ore formation and mineral exploration in epithermal system: A reconnaissance study at the Keyue and Zhaxikang Sb–Pb–Zn–Ag deposits in southern Tibet. Ore Geol. Rev. 139, 104594.
Wei, C., Huang, Z.L., Yan, Z.F., Hu, Y.S., Ye, L., 2018. Trace Element Contents in Sphalerite from the Nayongzhi Zn–Pb Deposit, Northwestern Guizhou, China: Insights into Incorporation Mechanisms, Metallogenic Temperature and Ore Genesis. Minerals 8, 490.
Wei, C., Huang, Z.L., Ye, L., Hu, Y.S., Santosh, M., Wu, T., He, L.L., Zhang, J.W., He, Z.W., Xiang, Z.Z., Chen, D., Zhu, C.W., Jin, Z.G., 2021. Genesis of carbonate–hosted Zn–Pb deposits in the Late Indosinian thrust and fold systems: An example of the newly discovered giant Zhugongtang deposit. South China. J. Asian Earth Sci. 220, 104914.
Wei, G.J., Huang, F., Ma, J.L., Deng, W.F., Yu, H.M., Kang, J.T., Chen, X.F., 2022. Progress of Non-Traditional Stable Isotope Geochemistry of the Past Decade in China. Bull. Mineral. Petrol. Geochem. 41 (1), 1–44. In Chinese with English abstract.
Wen, H.J., Carignan, J., Hu, R.Z., Fan, H.F., Chang, B., Yang, G.S., 2007. Large selenium isotopic variations and its implication in the Yutangba Se deposit, Hubei Province, China. Chin. Sci. Bullet. 52 (17), 2443–2447.
Wen, H.J., Zhang, Y.X., Fan, H.F., Hu, R.Z., 2009. Mo isotopes in the Lower Cambrian formation of southern China and its implications on paleo–ocean environment. Chinese Sci. Bull. 54, 4756–4762.
Wen, H.J., Zhu, C.W., Zhang, Y.X., Cloquet, C., Fan, H.F., Fu, S.H., 2016. Zn/Cd ratios and cadmium isotope evidence for the classification of lead–zinc deposits. Sci. Rep. 6, 25273.
Wen, H.J., Zhu, C.W., Du, S.J., Luo, C.G., 2020. Gallium (Ga), germanium (Ge), thallium (Tl) and cadmium (Cd) resources in China. Chin. Sci. Bull. 65 https://doi.org/10.1360/TB-2020-0267 (In Chinese with English abstract).
Wiggenhauser, M., Bigalke, M., Imseng, M., Müller, M., Keller, A., Murphy, K., Kreissig, K., Rehkämper, M., Wilcke, W., Frossard, E., 2016. Cadmium isotope fractionation in soil–wheat systems. Environ. Sci. Technol. 50 (17), 9223–9231.
Wu, Y., 2013. The age and ore−forming process of MVT deposit in the boundary area of Sichuan−Yunnan−Guizhou provinces, Southwest China. A Dissertation Submitted to China University of Geosciences for a Doctor Degree, Beijing (In Chinese with English abstract).
Wu, D.W., He, L.L., Cai, J,C., Wang, J., Bai, G.H., Yang, T., Jin, X.L., Huang Q., 2019. Main Orebody Characteristics and Ore−prospecting Symbols of Zhugongtang Lead-zinc Deposit in Hezhang, Guizhou. Guizhou Geol. 36(4), 299−306 (in Chinese with English abstract).
Wu, T., Huang, Z.L., He, Y.F., Yang, M., Fan, H.F., Wei, C., Ye, L., Hu, Y.S., Xiang, Z.Z., Lai, C., 2021. Metal source and ore–forming process of the Maoping carbonate–hosted Pb–Zn deposit in Yunnan, SW China: Evidence from deposit geology and sphalerite Pb–Zn–Cd isotopes. Ore Geol. Rev. 135, 104214.
Xie, R.C., Galer, S.J., Abouchami, W., Rijkenberg, M.J., de Baar, H.J., De Jong, J., Andreae, M.O., 2017. Non-Rayleigh control of upper-ocean Cd isotope fractionation in the western South Atlantic. Earth Planet. Sci. Lett. 471, 94–103.
Xu, C., Zhong, H., Hu, R.Z., Wen, H.J., Zhu, W.G., Bai, Z.J., Fan, H.F., Li, F.F., Zhou, T., 2020. Sources and ore–forming fluid pathways of carbonate–hosted Pb–Zn deposits in Southwest China: implications of Pb–Zn–S–Cd isotopic compositions. Miner. Deposita 55 (3), 491–513.
Yan, M.C., Chi, Q.H., 1997. THE CHEM ICAL COMPOSITIONS OF CRUST AND ROCKS IN THE EASTERN PART OF CHINA. Science Press, Beijing (in Chinese).
Yan, D.P., Zhou, M.F., Song, H.L., Wang, X.W., Malpas, J., 2003. Origin and tectonic significance of a Mesozoic multilayer overthrust system within the Yangtze Block (South China). Tectonophysics 361, 239–254.
Yang, J., Li, Y., Liu, S., Tian, H., Chen, C., Liu, J., Shi, Y., 2015. Theoretical calculations of Cd isotope fractionation in hydrothermal fluids. Chem. Geol. 391, 74–82.
Yang, C., Liu, S.A., Zhang, L., Wang, Z.Z., Liu, P.P., Li, S.G., 2021. Zinc isotope fractionation between Cr–spinel and olivine and its implications for chromite crystallization during magma differentiation. Geochim. Cosmochim. Acta 313, 277–294.
Yang, Z., Song, W.R., Wen, H.J., Zhang, Y.X., Fan, H.F., Wang, F., Li, Q.K., Yang, T., Zhou, Z.B., Liao, S.L., Zhu, C.W., 2022b. Zinc, cadmium and sulphur isotopic compositions reveal biological activity during formation of a volcanic–hosted massive sulphide deposit. Gondwana Res. 101, 103–113.
Yang, Q., Zhang, X.J., Ulrich, T., Zhang, J., Wang, J., 2022a. Trace element compositions of sulfides from Pb–Zn deposits in the Northeast Yunnan and northwest Guizhou Provinces, SW China: Insights from LA–ICP–MS analyses of sphalerite and pyrite. Ore Geol. Rev. 141, 104639.
Ye, L., Li, Z.L., Hu, Y.S., Huang, Z.L., Zhou, J.X., Fan, H.F., Danyushevskiy, L., 2016. Trace elements in sulfide from the Tianbaoshan Pb–Zn deposit, Sichuan Province, China: A LA–ICPMS study. Acta Petrol. Sin. 32 (11), 3377–3393. In Chinese with English abstract.
Ye, L., Wei, C., Hu, Y.S., Huang, Z.L., Li, Z.L., Yang, Y.L., Wang, H.Y., 2019. Geochemistry of germanium and its resources reserves. Mineral Deposits 38 (4), 711–728. In Chinese with English abstract.
Zhang, C.Q., 2008. The genetic model of Mississippi Valley–type deposits in the boundary area of Sichuan, Yunnan and Guizhou provinces, China. A dissertation submitted to Chinese Academy of Geological Sciences for a doctor degree, Beijing (In Chinese with English abstract).
Zhang, Y.X., Wen, H.J., Zhu, C.W., Fan, H.F., Luo, C.G., Liu, J., Cloquet, C., 2016. Cd isotope fractionation during simulated and natural weathering. Environ. Pollut. 216, 9–17.
Zhang, Y., Wen, H., Zhu, C., Fan, H., Cloquet, C., 2018. Cadmium isotopic evidence for the evolution of marine primary productivity and the biological extinction event during the Permian-Triassic crisis from the Meishan section, South China. Chem. Geol. 481, 110–118.
Zhang, C.Q., Wu, Y., Hou, L., Mao, J.W., 2015. Geodynamic setting of mineralization of Mississippi Valley–type deposits in world–class Sichuan–Yunnan–Guizhou Zn–Pb triangle, southwest China: Implications from age–dating studies past in the decade and the Sm–Nd age of Jinshachang deposit. J. Asian Earth Sci. 103, 103–114.
Zhou, J.X., Gao, J.G., Chen, D., Liu, X.K., 2013b. Ore genesis of the Tianbaoshan carbonate−hosted Pb–Zn deposit, Southwest China: geologic and isotopic (C–H–O–S–Pb) evidence. Int. Geol. Rev. 55 (10), 1300–1310.
Zhou, J., Huang, Z., Zhou, M., Li, X., Jin, Z., 2013a. Constraints of C-O–S−Pb isotope compositions and Rb–Sr isotopic age on the origin of the Tianqiao carbonate–hosted Pb–Zn deposit, SW China. Ore Geol. Rev. 53, 77–92.
Zhou, J.X., Huang, Z.L., Lv, Z.C., Zhu, X.K., Gao, J.G., Mirnejad, H., 2014a. Geology, isotope geochemistry and ore genesis of the Shanshulin carbonate–hosted Pb–Zn deposit, southwest China. Ore Geol. Rev. 63, 209–225.
Zhou, J.X., Bai, J.H., Huang, Z.L., Zhu, D., Yan, Z.F., Lv, Z.C., 2015. Geology, isotope geochemistry and geochronology of the Jinshachang carbonate–hosted Pb–Zn deposit, southwest China. J. Asian Earth Sci. 98, 272–284.
Zhou, J.X., Wang, X.C., Wilde, S.A., Luo, K., Huang, Z.L., Wu, T., Jin, Z.G., 2018. New insights into the metallogeny of MVT Zn–Pb deposits: A case study from the Nayongzi in South China, using field data, fluid compositions, and in situ S-Pb isotopes. Am. Miner. 103, 91–108.
Zhou, C.X., Wei, C.S., Guo, J.Y., 2001. The source of metals in the Qilingchang Pb–Zn deposit, Northeastern Yunnan, China: Pb–Sr isotope constraints. Econ. Geol. 96, 583–598.
Zhou, M.F., Yan, D.P., Kennedy, A.K., Li, Y.Q., Ding, J., 2002. SHRIMP U-Pb zircon geochronological and geochemical evidence for Neo-Proterozoic arc–related magmatism along the western margin of the Yangtze Block, South China. Earth Planet Sci. Lett. 196 (1–2), 51–67.
Zhou, J.X., Yang, Z.M., An, Y.L., Luo, K., Liu, C.X., Ju, Y.W., 2022. An evolving MVT hydrothermal system: Insights from the Niujiaotang Cd–Zn ore field, SW China. J. Asian Earth Sci. 237, 105357.
Zhou, M.F., Zhao, X.F., Chen, W.T., Li, X.C., Wang, W., Yan, D.Y., Qiu, H.N., 2014b. Proterozoic Fe–Cu metallogeny and supercontinental cycles of the southwestern Yangtze Block, southern China and northern Vietnam. Earth Sci. Rev. 139, 59–82.
Zhu, J.M., Tan, D.C., Wang, J., Zeng, L., 2015. Application and progress in selenium stable isotope geochemistry. Earth Sci. Front. 22 (5), 102–114. In Chinese with English abstract.
Zhu, X.K., Wang, Y., Yan, B., Li, J., Dong, A.G., Li, Z.H., Sun, J., 2013a. Developments of Non-Traditional Stable Isotope Geochemistry. Bull. Mineral. Petrol. Geochem. 32 (6), 651–688. In Chinese with English abstract.
Zhu, C.W., Wen, H.J., Zhang, Y.X., Fan, H.F., Fu, S.H., Xu, J., Qin, T.R., 2013b. Characteristics of Cd isotopic compositions and their genetic significance in the lead–zinc deposits of SW China. Sci. China Earth Sci. 56 (12), 2056–2065.
Zhu, C.W., Wen, H.J., Zhang, Y.X., Fan, H.F., 2016. Cadmium and sulfur isotopic compositions of the Tianbaoshan Zn–Pb–Cd deposit, Sichuan Province. China. Ore Geol. Rev. 76, 152–162.
Zhu, C.W., Wen, H.J., Zhang, Y.X., Fu, S.H., Fan, H.F., Cloquet, C., 2017. Cadmium isotope fractionation in the Fule Mississippi Valley–type deposit. Southwest China. Miner. Deposita 52 (5), 675–686.
Zhu, C.W., Wen, H.J., Zhang, Y.X., Huang, Z.L., Cloquet, C., Luais, B., Yang, T., 2021. Cadmium isotopic constraints on metal sources in the Huize Zn–Pb deposit. SW China. Geosci. Front. 12 (6), 101241.